Chemistry and Physics of Lipids 219 (2019) 36–44

Contents lists available at ScienceDirect

Chemistry and Physics of Lipids

journal homepage: www.elsevier.com/locate/chemphyslip

# Fibrillation mechanism of glucagon in the presence of phospholipid bilayers as revealed by $^{13}C$ solid-state NMR spectroscopy

Izumi Yamane, Ayano Momose, Hideki Fujita, Eri Yoshimoto, Akie Kikuchi-Kinoshita, Izuru Kawamura, Akira Naito*

*Graduate School of Engineering, Yokohama National University, 79-5 Tokiwadai, Hodogaya-ku, Yokohama, 240-8501, Japan*

ARTICLE INFO

*Keywords:*
Glucagon
Phospholipid bilayers
Bicelle
Fibrillation mechanism
Fibrillation kinetics
$^{13}C$ solid-state NMR

ABSTRACT

Glucagon is a 29 amino acid peptide hormone secreted by pancreatic α−cells and interacts with specific receptors located in various organs. Glucagon tends to form gel-like fibril aggregates that are cytotoxic because they activate apoptotic signaling pathways. To understand mechanism of fibril formation, we investigated the structure and kinetics of glucagon fibril formation using $^{13}C$ solid-state NMR spectroscopy. In aqueous acetic acid solution at pH 3.3, distorted α−helical structure appeared around Gly4, Leu14, Ala19 and Leu26 in the monomeric form. In contrast, Gly4 and Ala19 were involved in β-sheet structures in the fibril form. The fibrillation process can be explained by a two-step autocatalytic reaction mechanism in which the first step is a homogeneous nuclear formation ($k_1$), and the second step is an autocatalytic heterogeneous fibrillation process ($k_2$). The rate constants $k_1$ and $k_2$ were separately determined in the acetic acid solution. Fibril formation was further investigated in the presence of lipid bilayers to mimic the physiological condition. We used bicelles which form discoidal nano-particles as the bilayer system and observed that the N-terminal α-helix did not change to β-sheet when fibrils formed in the presence of bicelles. Rate constant $k_1$ became faster and $k_2$ became slower in the presence of bicelles compared to the case in the absence of bicelles. Our findings reveal that the structure and kinetics of fibril formation by glucagon are altered in the presence of lipid bilayers.

## 1. Introduction

Glucagon is a 29 amino acid peptide hormone secreted by pancreatic α−cells which interacts with specific receptors located in various organs, especially the liver, where it plays a crucial role in glucose homeostasis in mammals (Bromer et al., 1957; Pohl et al., 1969; Rodbell et al., 1971). The primary structure of glucagon peptide is as follows.

$His^{1}$-Ser-Gln-Gly-$Thr^{5}$-Phe-Thr-Ser-Asp-$Tyr^{10}$-Ser-Lys-Tyr-Leu-$Asp^{15}$-Ser-Arg-Arg-

Ala-$Gln^{20}$-Asp-Phe-Val-Gln-$Trp^{25}$-Leu-Met-Asn-Thr-OH.

Glucagon tends to form gel-like fibrillar aggregate (Beaven et al., 1969) which exhibit cytotoxicity through the activation of apoptotic signaling pathways (Onoue et al., 2004). Glucagon forms fibrils similar to that of other therapeutic peptides such as human calcitonin (Kamgar-Parsi et al., 2017a) and insulin (Burke and Rougvie, 1972) and pathologically related fibrils such as prion (Prusiner, 1998), amylin (type 2 diabetic patients) (Cooper et al., 1987), β−amyloid (Alzheimer's disease) (Vines, 1993), and polyglutamine (Scherzinger et al., 1997).

The formation of polymerized insoluble amyloid fibrils from normally innocuous, soluble proteins or peptides has been observed under biochemically diverse conditions. A number of non fibrillar proteins or peptides have been identified to form amyloid fibrils that exhibit similar morphologies as observed from electron micrographs (Sipe, 1992). Several phenomena associated with fibrils are related to the misfolding of proteins, leading to severe diseases such as fibril deposit in the brain of Alzheimer's disease patients (Sipe and Cohen, 2000) and in the pancreas of patients with type II diabetes (Cooper et al., 1987).

Kinetic analyses of fibril formation by the therapeutic peptide human calcitonin (hCT) indicate that hCT molecules associate to form fibril intermediates via a two-step autocatalytic reaction mechanism. The first step kinetic reaction (rate constant, $k_1$) is a homogeneous reaction to form fibril intermediates and the resulting intermediates react with monomeric molecules to elongate into longer fibrils via a heterogeneous fibril elongation process (rate constant, $k_2$) (Kamihira et al., 2000; Itoh-Watanabe et al., 2013a, b; Kamgar-Parsi et al., 2017b). Elucidating the molecular structure of amyloid fibrils is important for understanding the mechanism of self-aggregation, but it is difficult to

* Corresponding author.
*E-mail address:* naito@ynu.ac.jp (A. Naito).

https://doi.org/10.1016/j.chemphyslip.2019.01.008
Received 16 October 2018; Received in revised form 23 January 2019; Accepted 23 January 2019
Available online 25 January 2019
0009-3084/ 

determine high-resolution molecular structure using typical spectroscopic methods because fibrils are heterogeneous solids. Solid-state NMR spectroscopy has demonstrated advantages for the conformational determination of Alzheimer's amyloid β−peptides (Aβ), which comprise 39–42 amino acids residues and are the main component of the amyloid plaques found in Alzheimer's disease patients (Sipe, 1992; Gorman and Chakrabartty, 2001). Both the intra-chain conformation of the Aβ molecule in fibrils and its intermolecular alignment have been analyzed to explore the mechanism of molecular association underlying the formation of Aβ (1–40) (Tycko, 2003a, b; Petkova et al., 2006) and the more toxic Aβ (1–42) (Xiao et al., 2015; Wälti et al., 2016; Colvin et al., 2016) fibrils.

An X-ray crystallographic study showed that glucagon adopts a trimer α−helix structure stabilized by hydrophobic interactions between molecules related by threefold symmetry (Sasaki et al., 1975). Glucagon in dilute aqueous solution may not form a specific structure with the exception of the 22–25 region as investigated by solution NMR studies (Boesch et al., 1978). The secondary structure of glucagon in the presence of dodecylphosphocholine micelles comprises three turns of an irregular α-helix formed by residues 17 to 29 near the C terminus, a stretch of extended polypeptide chain from residues 14 to 17, an α-helix-like turn formed by residue 10 to 14 and another extended region from residue 5 to 10 (Braun et al., 1983).

Fibril formation by glucagons was observed by Beaven et al. in undisturbed aqueous solution at pH 2: with time, the viscosity increased and a birefringent gel formed. On further standing, a precipitate appeared comprising long fibrils, as determined using electron microscopy (Beaven et al., 1969). Infrared spectra of the gel, solid film and precipitate showed that glucagon fibrillar aggregates produced in the acidic condition formed antiparallel β−sheet chains and these glucagon aggregates displayed significant cytotoxity (Onoue et al., 2004, 2006). Kinetic analysis of fibril formation by glucagon under acidic conditions demonstrated a complex fibrillation mechanism in which suitable changes in the fibrillation condition can alter the type of fibril formed or result in the formation of a mixture of several types of fibrils (Pedersen et al., 2006). Furthermore, the fibrils come in two forms: one composed entirely of glucagon monomers and one entirely of glucagon trimers (Košmrlj et al., 2015).

Understanding the cytotoxicity of amyloid forming peptides, requires investigation of the interaction of peptides with membrane because lipid bilayer components dramatically alter most aspect of amyloid aggregation (Naito and Kawamura, 2007; Brender et al., 2012; Kotler et al., 2014; Matsuzaki, 2014; Kael et al., 2018; Okada et al., 2018).

In this study, we analyzed the kinetic behavior of glucagons in aqueous solution in the presence and absence of lipid bilayers to understand the fibrillation process under physiological condition. In the lipid bilayer systems, bicelles can be used to investigate glucagon membrane interaction to affect the fibril formation. Bicelles composed of 1,2-dimyristoyl-sn-glycero-3-phosphocholine (DMPC) and 1,2-dihexanoyl-sn-glycero-3-phosphocholine (DHPC) are most frequently used (Sanders and Schwonek, 1992). In fact, transmembrane structure and topology of microsomal cytochrome-P450 were revealed by solid-state NMR using temperature-resisted bicelles (Yamamoto et al., 2013). In the study of P450, although bicelles rendered far more stability for active P450 than micelles, it was limited for stability for active P450, because detergent or short-chain lipids surrounding like a belt of the planer lipid bilayer in bicelles diffuse to deactivate P450 (Bamaba and Ramamoorthy, 2018).

Nanodiscs are lipid bilayer particles surrounded by an amphiphilic belt which inspiration from plasma lipoprotein (Denisov and Sligar, 2017). Since there are no detergents diffuse to lipid bilayer area and thus include high versatility in lipid composition. The membrane-scaffold protein (MSP) nanodiscs were first introduced, and MSP and its derivative spontaneously form nanodiscs with several phospholipids, being DMPC and 1-palmitoyl-2-oleoyl-sn-glycero-3-phosphocholine (POPC) nanodiscs the most used for structural studies of proteins interacted with membrane. Peptide-based nanodiscs are used to investigate protein-protein interaction (Zhang et al., 2016; Sahoo et al., 2018a). Polymer-based nanodiscs are also used to study membrane proteins in the membrane environments (Knowles et al., 2009; Bersch et al., 2017; Ravula et al., 2018). Consequently, β-amyloid aggregate kinetics and structure changes in the presence of polymethacrylate-copolymer (PMA) encoded lipid-nanodiscs (Sahoo et al., 2018b) and ganglioside GM1 containing nanodiscs (Thomaier et al., 2016), respectively. Amyloid aggregation of human-IAPP were studied in the presence of MSP based nanodiscs (Camargo et al., 2017).

## 2. Materials and methods

### 2.1. Materials

Four types of $^{13}$C-labeled and non-labeled glucagon molecules were synthesized using Fmoc chemistry on an Applied Biosystems 431 A peptide synthesizer: wild type (WT)-glucagon, with the natural isotope abundance, [1-$^{13}$C]Gly4, [3-$^{13}$C]Ala19-glucagon, [1-$^{13}$C]Phe6-glucagon, [1-$^{13}$C]Leu14-glucagon and [1-$^{13}$C]Leu26-glucagon. Fmoc $^{13}$C-labeled amino acids (99% enriched) were synthesized by reacting Fmoc-Osu with [1-$^{13}$C] or [3-$^{13}$C]-labeled amino acids (from CIL, Andover, Massachusetts) following the method of Paquet (Paquet, 1982). The synthesized peptides were purified by reversed-phase high-performance liquid chromatography (HPLC) using a mixture of water and acetonitrile containing 0.05% TFA as the mobile phase after deprotection and cleavage from the resin.

Fibril formation was observed with time by dissolving each glucagon in 0.015 M acetic acid solution (18 mg/mL) at pH 3.3. Acidic solution was chosen to resolved glucagon in the concentration of 18 mg/mL. A portion of the solution (80 μL) was immediately placed in a 5 mm-o.d. zirconia rotor for the solid-state $^{13}$C NMR studies and sealed with Araldite to prevent evaporation of the mother liquor during the NMR measurements. Bicelles were prepared by mixing phospholipids, DMPC and DHPC, in a molar ratio of 3:1 in 0.015 M acetic acid solution then the bicelles and each glucagon were mixed at a molar ratio of glucagon : phospholipid = 1 : 5. This large glucagon ratio to phospholipid is chosen to observe $^{13}$C NMR signals of glucagon in the bicelle containing solution. Disc shaped bicelles with diameter of 20–50 nm were observed in the acidic solution (Fig. 1D) and in the presence of glucagon (Fig. 1E). This sample was placed in a 5 mm o.d. zirconia rotor for the solid-state $^{13}$C NMR measurements of glucagon fibril formation in the presence of lipid bilayers.

### 2.2. $^{13}$C Solid-state NMR measurements

All $^{13}$C NMR spectra were recorded on a Chemagnetics CMX 400 Infinity NMR spectrometer at a resonance frequency of 100.6 MHz for $^{13}$C and 398.6 MHz for $^{1}$H. $^{13}$C NMR spectra were obtained using CP-MAS (combination of cross-polarization, high-power dipolar decoupling, and magic-angle spinning) and DD-MAS (combination of 90° pulse excitation, high power proton dipolar decoupling, and magic angle spinning) techniques. The CP-MAS method (Schaefer and Sejeskal, 1976) provides signals of the solid component (fibril), and the DD-MAS method primarily provides signals from the solution components (monomer for the carbonyl carbons and both monomer and fibril components for the methyl carbons based on their spin-lattice relaxation times compared with repetition times). The duration of 90° pulses for $^{13}$C and $^{1}$H nuclei were 5.5 μs, the contact time for CP-MAS experiments was 1.0 ms, the repetition time was 4 s, and the MAS frequency of 4 kHz was used. In the Fourier transformation, line broadening values of 20 and 30 Hz were used for DD-MAS and CP-MAS experiments, respectively. The $^{13}$C chemical shifts were calibrated using the external carboxyl peak of crystalline glycine at 176.03 ppm from tetramethylsilane (TMS). All NMR measurements were performed at

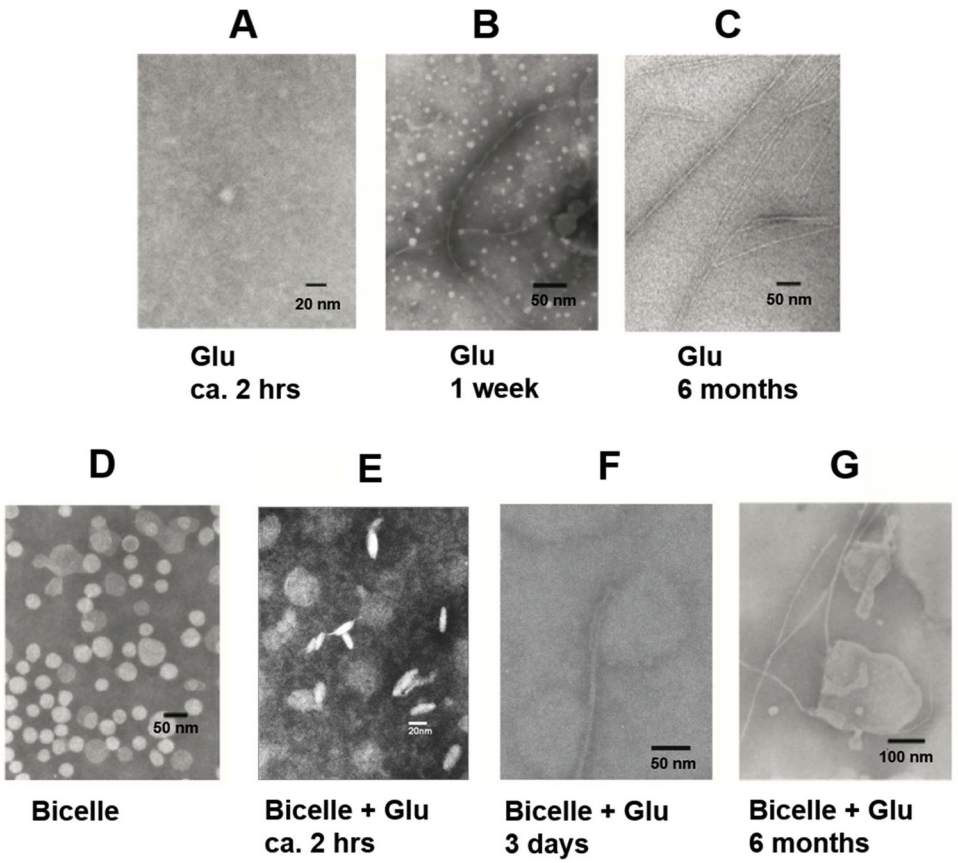


**Fig. 1.** Transmission electron micrographs of glucagon (18 mg/mL) in 0.015 M acetic acid solution at pH 3.3. (A) Taken at ca. 2 h after dissolution of glucagon. Bar indicates 20 nm. (B) Taken at 1 week after dissolution of glucagon. Bar indicates 50 nm. (C) Taken at 6 months after dissolution of glucagon. Bar indicates 50 nm. (D) TEM picture of bicelles in 0.015 M acetic acid solution at pH 3.3. Bar indicates 50 nm. (E) Taken at ca. 2 h after dissolution of glucagon in the presence of bicelles. Bar indicates 20 nm. (F) Taken at 3 days after dissolution of glucagon in the presence of bicelles. Bar indicates 50 nm. (G) Taken at 6 months after dissolution of glucagon in the presence of bicelles. Bar indicates 100 nm.

20 °C. The temperature of 20 °C is chosen to reduce the hydrolysis of lipid molecules by maintaining lipid bilayer state in the acetic acid solution at pH 3.3. The numbers of accumulations in the time-course study for the DD- and CP-MAS signals were 1000 and 2000, respectively, and the two methods were used alternately to observe the fibrillation process and to determine the rate constants of the two-step autocatalytic reaction mechanism (Kamihira et al., 2000).

### 2.3. TEM measurements

Glucagon containing solutions in the absence and presence of bicelles were prepared as the same procedures as used for NMR measurements and were staying statically at room temperature (ca. 20 °C). 1μl of glucagon suspension was diluted with 500 fold HEPES solution and placed on hydrophilic grid. Subsequently, 5μl of 3% phosphotungstic acid solution at pH 4 was added and stained for 10 s. The negatively stained samples were measured using JEOL 1200EX II transmission electron microscope (TEM) operating at 80 kV.

## 3. Results

### 3.1. Characterization of glucagon fibril in the presence and absence of bicelles

Fig. 1A–C show TEM pictures of a pH 3.3 acetic acid solution which were measured at ca. 2 h after dissolution of glucagon, 1 week after dissolution and 6 months after dissolution, respectively. At ca. 2 h after dissolution of glucagon, small number of spherical shape of fibril intermediates appeared as shown in Fig. 1A. At 1 week after dissolution of glucagon, a number of spherical fibril intermediates increased and elongated fibrils were also appeared (Fig. 1B). Similar spherical fibril intermediates have been observed in the case of hCT in HEPES solution (Itoh-Watanabe et al., 2013b) and β-amyloid (Chimon et al., 2007). At 6 months after dissolution of glucagon, Long matured fibrils about 10 nm diameter were observed and spherical fibril intermediates completely disappeared (Fig. 1C).

Fig. 1D shows TEM picture of pH 3.3 acetic acid bicelle solution without glucagon. This result confirmed that lipid-bilayer bicelles are formed in acidic solution at 20 °C. A number of discoidal bicelles with the diameter of 20–50 nm were seen. Fig. 1E–G show TEM pictures of a pH 3.3 acetic acid solution of glucagon in the presence of bicelles which were measured at ca. 2 h after dissolution of glucagon, 3 days after dissolution of glucagon, and 6 months after dissolution, respectively. At ca. 2 h after mixing glucagon, disc shaped bicelles with approximately 40 nm diameter appeared together with ellipsoid shaped glucagon aggregates (Fig. 1E). These fibril aggregates may correspond to fibril intermediates comprising glucagon fibril nuclei similar to that observed for hCT in HEPES solution (Itoh-Watanabe et al., 2013b) and β-amyloid (Chimon et al., 2007). At 3 days after mixing glucagon, long fibrils had grown by attaching to the edge of the bicelles and ellipsoid shaped glucagon aggregates had disappeared (Fig. 1F). At 6 months after mixing glucagon, the bicelles had fused to make larger bicelles and glucagon fibrils were observed on the edge of the bicelles (Fig. 1G). This result suggests that glucagon fibrils interact with the bicelles during the nucleation and fibril elongation processes.

### 3.2. $^{13}C$ NMR spectra of site-specifically $^{13}C$-labeled glucagons

$^{13}C$ DD-MAS signals indicate monomer or micelle states of glucagon and $^{13}C$ CP-MAS signals indicate fibril state though two different morphological states are mixed in the solution of glucagon. Fig. 2 shows $^{13}C$ DD- and CP-MAS NMR spectra of monomers and fibrils of the site specifically $^{13}C$-labeled glucagons, [1-$^{13}C$]Gly$^{4}$, [3-$^{13}C$]Ala$^{19}$-glucagon and [1-$^{13}C$]Leu14 and [1-$^{13}C$]Leu26-glucagon molecules of the monomers (DD-MAS) and fibrils (CP-MAS) in pH 3.3 acetic acid solution. The DD-MAS spectra (Fig. 2A and C) of [1-$^{13}C$]Gly4 and [3-$^{13}C$]Ala19

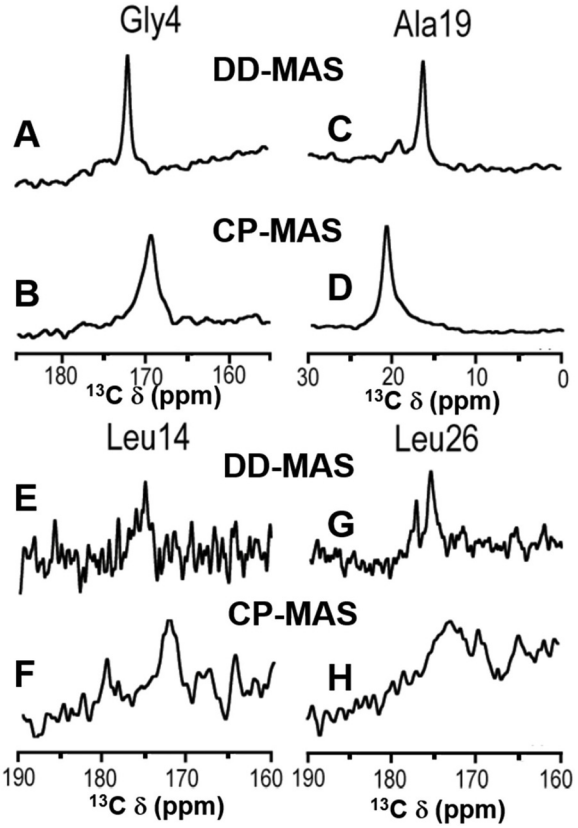


**Fig. 2.** $^{13}$C DD-MAS and CP-MAS NMR spectra of [1-$^{13}$C]Gly4 (A, B), [3-$^{13}$C]Ala19 (C, D), [1-$^{13}$C]Leu14 (E, F) and [1-$^{13}$C]Leu26 (G, H) in acetic acid solution at pH 3.3.

**Table 1**
Structural transitions during glucagon fibrillation as determined by conformation-dependent $^{13}$C chemical shifts (ppm)*.

| | Absence of bicelles | | Presence of bicelles | |
|---|---|---|---|---|
| | monomer | fibril | monomer | fibril |
| Gly$^{4}$ | 171.7 ± 0.3 (α-helix) | 169.2 ± 0.4 (β-sheet) | 171.5 ± 0.2 (α-helix) | 171.5 ± 0.3 (α-helix) |
| Phe$^{6}$ | 173.5 ± 0.3 (random coil) | 172.1 ± 0.4 (random coil) | 173.7 ± 0.3 (random coil) | 173.7 ± 0.4 (random coil) |
| Leu$^{14}$ | 175.3 ± 0.6 (α-helix) | 172.2 ± 1.0 (random coil) | 174.0 ± 0.3 (random coil) | 172.5 ± 0.4 (random coil) |
| Ala$^{19}$ | 16.4 ± 0.3 (α-helix) | 21.0 ± 0.3 (β-sheet) | 16.4 ± 0.3 (α-helix) | 19.3 ± 0.4 (β-sheet) |
| Leu$^{26}$ | 175.7 ± 0.3 (α-helix) | 172.9 ± 1.4 (random coil) | 175.7 ± 0.6 (α-helix) | 173.1 ± 1.4 (random coil) |

* The structure around each amino acid residues was determined by comparing the experimentally obtained $^{13}$C chemical shift values ($\delta_{iso}$) values with typical $^{13}$C chemical shift values ($\delta_{iso}$) of (α-helix, β-sheet), which are reported as (171.6, 168.5), (175.1, 170.6) and (175.7, 170.2) for [1-$^{13}$C]Gly, [1-$^{13}$C]Phe and [1-$^{13}$C]Leu, and (14.9, 19.9) for [3-$^{13}$C]Ala, respectively (Saitô, 1986; Saitô and Ando, 1989; Saitô et al., 2010).

exhibit the signals at 171.7 and 16.4 ppm, for the carbonyl carbon and methyl carbon, respectively, of the monomeric state, indicating that the region near Gly4 and Ala19 form distorted α−helix structure as shown in the conformation-dependent chemical shift values (Saitô, 1986; Saitô and Ando, 1989; Saitô et al., 2010) and experimentally determined chemical shifts summarized in Table 1. Secondary structures around the $^{13}$C labelled amino acid residues of glucagon were estimated from these experimentally determined chemical shifts and typical conformation dependent chemical shifts and are also summarized in Table 1.

The $^{13}$C CP-MAS spectra of [1-$^{13}$C]Gly4 and [3-$^{13}$C]Ala19 (Fig. 2B and D) of the fibril state shows relatively broad peaks at 169.2 and 21.0 ppm for the carbonyl (Gly4) and methyl (Ala19) carbons, respectively. Given the conformation-dependent chemical shift values (Table 1), these chemical shifts indicate that the vicinities of Gly4 and Ala19 form β−sheet structures, showing that the N-terminus and C-terminus of these glucagon molecules change from an α−helix to a β−sheet structure when the monomers form fibrils. [1-$^{13}$C]Leu14 exhibits peaks at 175.3 and at 172.2 ppm for monomers (DD-MAS) and fibrils (CP-MAS), respectively (Fig. 2E and F), similarly indicating that the vicinity of Leu14 changes structure from an α−helix to a random coil upon fibril formation. Similarly, [1-$^{13}$C]Leu26 exhibit peaks at 175.7 and 172.9 ppm for monomers (DD-MAS) and fibrils (CP-MAS), respectively (Fig. 2G and H, and Fig. S4), similarly indicating that the vicinity of Leu26 changes structure from an α−helix to a random coil. Leu26 may adopt a random coil structure due to its proximity to the C-terminal region (Table 1). [1-$^{13}$C]Phe6 exhibit peaks at 173.5 and 172.1 ppm for monomers and fibrils, respectively, indicating that the vicinity of Phe6 maintains random coil in the absence of bicelles (Table 1).

Fig. 3A and C, and Fig. S1 shows the DD-MAS spectra of [1-$^{13}$C]Gly4, [3-$^{13}$C]Ala19-glucagon in the presence of bicelles at pH 3.3. The two signals at 171.5 and 16.4 ppm, for the carbonyl carbon (Gly4) and methyl carbon (Ala19), respectively, indicating that the vicinities of both Gly4 and Ala19-glucagon form α−helical structures in monomers based on conformation-dependent chemical shift values (Table 1). The $^{13}$C CP-MAS spectra of [1-$^{13}$C]Gly4, [3-$^{13}$C]Ala19-glucagons in the presence of bicelles (Fig. 3B and D, and Fig. S1) show relatively broad peaks at 171.5 and 19.3 ppm for the carbonyl (Gly4) and methyl (Ala19) carbons, respectively, indicating that the vicinities of Gly4 and Ala19 form respectively α−helix and β−sheet structures.

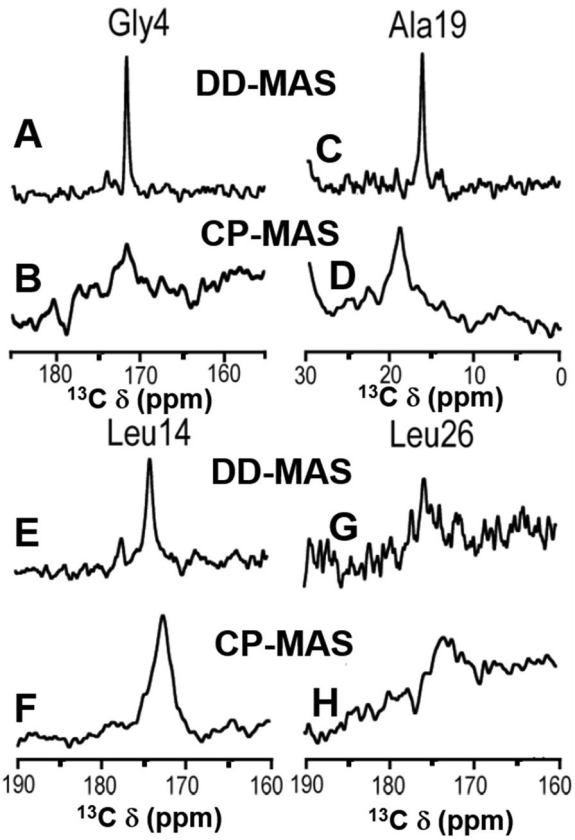


**Fig. 3.** $^{13}$C DD-MAS and CP-MAS NMR spectra of [1-$^{13}$C]Gly4 (A, B), [3-$^{13}$C]Ala19 (C, D), [1-$^{13}$C]Leu14 (E, F) and [1-$^{13}$C]Leu26 (G, H) in acetic acid solution in the presence of bicelles at pH 3.3.

It is noted that the N-terminus did not undergo a change in α-helix structure, while the C-terminus changed from an α-helix to a β−sheet when the monomers formed fibrils in the presence of bicelles. As shown in Fig. 3E and F, Fig. S2 and Table 1 [1-$^{13}$C]Leu14 exhibits peaks at 174.0 and 172.2 ppm for monomers (DD-MAS) and fibrils (CP-MAS), respectively, in the presence of bicelles, indicating that the region around Leu14 changes structure from a distorted α−helix to a random coil during fibril formation in the presence of bicelles. Similarly, [1-$^{13}$C] Leu26 (Fig. 3G and H, and Fig. S3) exhibit a peak at 175.7 and 173.1 ppm for monomers (DD-MAS) and fibrils (CP-MAS), respectively, indicating that the vicinity around Leu26 changes from an α−helix to a random coil in the presence of bicelles. Leu26 may adopt a random coil structure due to its proximity to the C-terminus. [1-$^{13}$C]Phe6 exhibit peaks at 173.5 and 172.1 ppm for monomers and fibrils, respectively, indicating that the vicinity of Phe6 maintains random coil in the presence of bicelles (Table 1).

### 3.3. Time-course behavior of glucagon fibrillation

We determined the kinetic properties of the conformational transition during the glucagon fibrillation process from time-course variations in the signal intensities, as shown in Fig. 4 for [1-$^{13}$C]Gly4-glucagon and Fig. 5 for [3-$^{13}$C]Ala19-glucagon. Variations in signal intensities for the monomer (DD-MAS signals) and fibril states (CP-MAS signals) can be observed separately in the same sample because the DD-MAS and CP-MAS NMR signals correspond to the monomer and fibril states of glucagon, respectively. Acquisition of the $^{13}$C DD- and CP-MAS spectra at 20 °C was initiated 6 h after dissolving 18 mg/mL [1-$^{13}$C]Gly4, [3-$^{13}$C]Ala19-glucagon in 0.015 M acetic acid solution (pH 3.3) because 6 h was required to tightly seal the sample rotor using glue. In the absence of bicelles, the signal intensities of the $^{13}$C DD-MAS spectra decreased gradually with time up to 42 h and significantly decreased after 66 h while those of the $^{13}$C CP-MAS spectra increased gradually with time up to 43 h as the fibrils grew and significantly increased after 67 h (left side of Figs. 4 and 5). In the presence of bicelles, the signal intensities of the $^{13}$C DD-MAS spectra decreased gradually up to 52 h and significantly decreased after 112 h, while those of $^{13}$C CP-MAS spectra increased gradually up to 53 h and significantly increased after 113 h (right side of Figs. 4 and 5). In contrast, the line position and shapes of the $^{13}$C DD- and CP-MAS signals for the [1-$^{13}$C]Gly4 and [3-$^{13}$C]Ala19 residues did not vary throughout the fibrillation process (Figs. 4 and 5). indicating that the conformations of the glucagon monomers and fibrils remain unchanged but only quantities of monomers and fibrils were changed during the fibril formation.

As shown in Fig. 6, plots of the resonance intensities of the CP-MAS spectra of the [1-$^{13}$C]Gly4 and [3-$^{13}$C]Ala19 residues against elapsed time in the acetic acid solution (red line) show that the carbonyl (Gly4) and methyl (Ala19) signals in the CP-MAS spectra increased gradually following a certain delay time for 30 h, as shown by the red line in Fig. 6. Then signal intensities increased rapidly up to 47 h following dissolution of glucagon. After 60 h, fibril formation was almost completed. Plots of the signal intensities of the CP-MAS spectra of [1-$^{13}$C]Gly4 and [3-$^{13}$C]Ala19-glucagon in the presence of bicelles against elapsed time are shown as blue line in Fig. 6. These signal intensities increase gradually during a certain delay time, but more rapidly increased than in the absence of bicelles during the initial stage up to 30 h. After 30 h this increased rate eventually became slower than in the absence of bicelles. It is, therefore, apparent that the glucagon fibril formation rate after a certain delay time is slower in acetic acid solution in the presence of bicelles than that in the absence of bicelle.

### 3.4. Kinetic analysis of the glucagon fibrillation process

We determine the rate constants of glucagon fibril formation by observing the signal intensities in the $^{13}$C CP-MAS NMR spectra with elapsed time (Fig. 6). The signal intensities of [1-$^{13}$C]Gly4 and [3-$^{13}$C]Ala19-glucagons increased after a certain delay time. The increase in $^{13}$C CP-MAS signal intensity corresponds to the increase in fibril components and thus we analyzed the rate constants, $k_1$ and $k_2$, of the two-step autocatalytic reaction mechanism, in which $k_1$ is the rate constant for fibril nucleation process and $k_2$ indicate rate constant for fibril elongation processes (Fig. 7) as reported in the previous study (Kamihira et al., 2000).

In the kinetic analysis, we assume that $n_0$ number of glucagon monomer (A) forms micelle with $n_0$ number ($A_{n0}$) as a solubilized process in the solution.

$$n_0A \text{ (monomer)} \rightleftarrows A_{no} \text{ (micelle)} \quad (1)$$

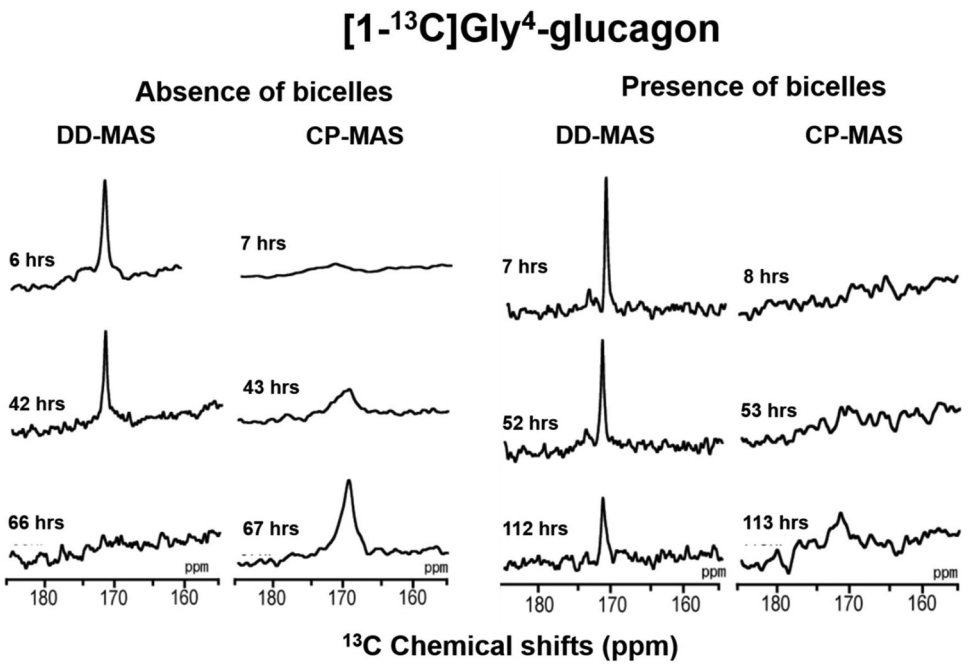


**Fig. 4.** Time course of $^{13}$C CP-MAS and DD-MAS signal intensities of [1-$^{13}$C]Gly4-glucagon during the fibril formation process.

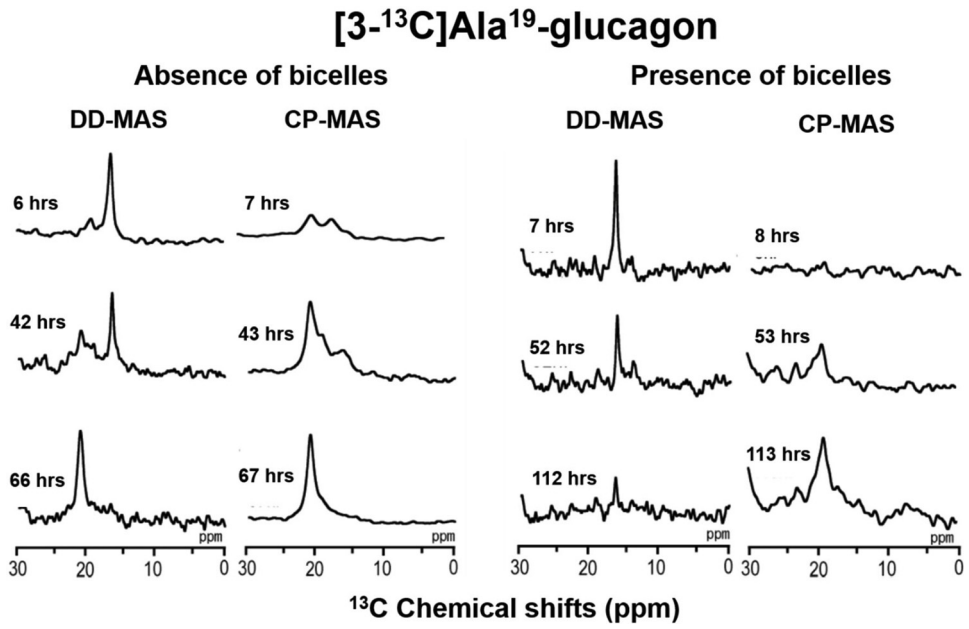


**Fig. 5.** Time course of $^{13}$C CP-MAS and DD-MAS signal intensities of [3-$^{13}$C]Ala19-glucagon during the fibril formation process.

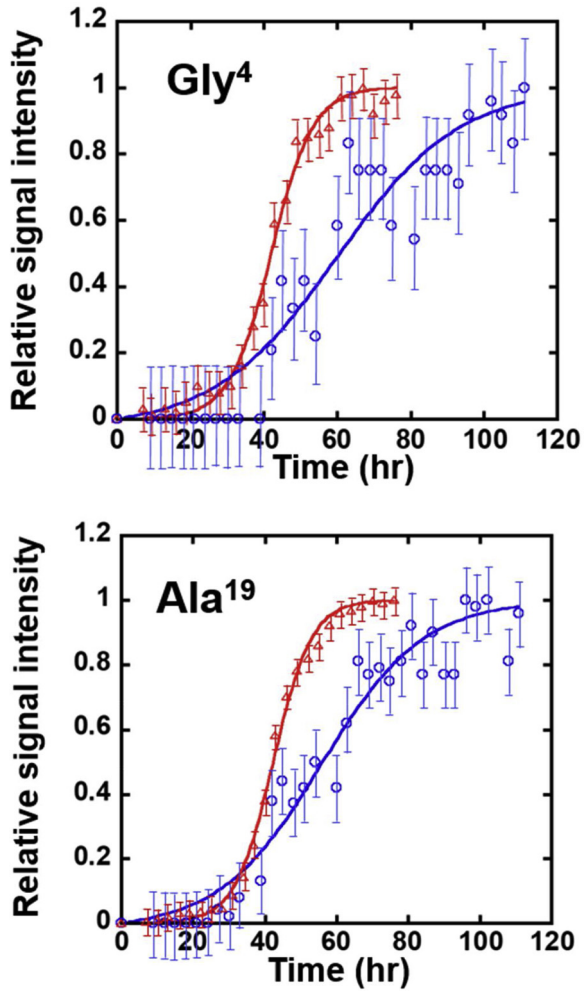


**Fig. 6.** Plots of relative signal intensities of [1-$^{13}$C]Gly4 and [3-$^{13}$C]Ala19 in $^{13}$C CP-MAS NMR spectra obtained in acetic acid solution (red line) and in acetic acid solution in the presence of bicelles (blue line) at pH 3.3. Vertical bars indicate error range.

Naturally, we assume that glucagon in the monomer and micelle states show the same structure. The first rate-determining reaction step is the nuclear formation step and can be given by

$$A_{no} \xrightarrow{k_1} B_{no} \quad (2)$$

where $A_{no}$ is micelles formed by an $n_o$ number of A form glucagon monomer molecules and $B_{no}$ is fibril intermediates (fibril nucleus) formed by an $n_o$ number of B form glucagon fibril molecules. The kinetic equation for Reaction (2) can be given by

$$(df/dt)_1 = k_1(1\text{-}f) \quad (3)$$

where f is the fraction of B form molecules in the system.

The second heterogeneous fibril elongation reaction can be given by

$$A + B_n \xrightarrow{k_2} B_{n+1} \quad (4)$$

where $B_n$ and $B_{n+1}$ are elongated fibrils with n and n+1 number of B form glucagon molecules. The relevant kinetics equation is given by

$$(df/dt)_2 = k_2af(1\text{-}f) \quad (5)$$

where, a is the initial concentration of glucagon. The overall kinetic equation can be given by

$$(df/dt) = (df/dt)_1 + (df/dt)_2 = k_1(1\text{-}f) + k_2a(1\text{-}f) \quad (6)$$

Eq. (6) can be integrated to give

$$f = \frac{\rho\{\exp[(1+\rho)kt] - 1\}}{\{1 + \rho\exp[(1+\rho)kt]\}} \quad (7)$$

where, f is the fraction of glucagon molecules in the fibril form at time t, ρ represents a dimensionless value describing the ratio of $k_1$ (the rate constant for the first nucleation process) to k, namely $\rho = k_1/k$ and $k = ak_2$ ($k_2$ is the rate constant for the second elongation process of the fibrils, and a is the initial peptide concentration) (Kamihira et al., 2000). The best fits of Eq. (7) are shown in Fig. 6 (solid lines) and analyzed rate constants are summarized in Table 2. Experimentally, $k_1$ and $k_2$ values were obtained from intensity variation of $^{13}$C CP-MAS NMR signals of [1-$^{13}$C]Gly4 and [3-$^{13}$C]Ala19 as shown in Fig. 6 and Table 2. Because time course behavior of [1-$^{13}$C]Gly4 and [3-$^{13}$C]Ala19 should be the same, rate constants obtained from Gly4 and Ala19 were further averaged to get averaged rate constants (Av. RC) which reasonably reflect glucagon fibrillation process (Table 2). Notably, $k_1$

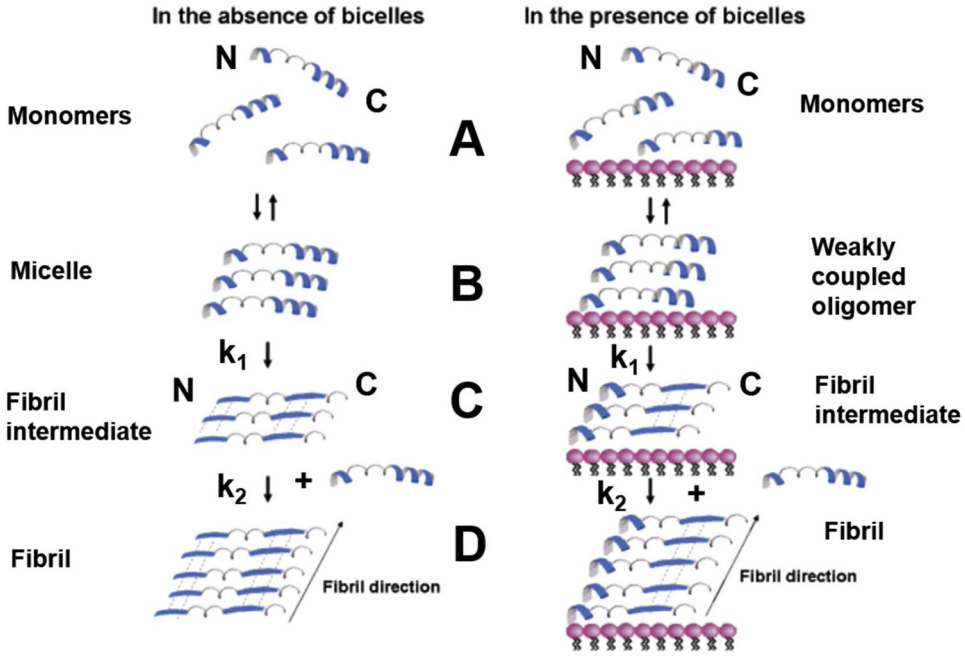


**Fig. 7.** Schematic diagram of fibrillation process of glucagon in acetic acid solution in the absence of bicelles (Left side) and in the presence of biclelles (Right side). (A) Schematic diagram of monomer form of glucagon. The N- and C-terminal regions of monomeric glucagon molecules form α-helices. (B; left side): The monomers associate with each other to form micelles. (B; right side): In the presence of a lipid bilayer, glucagon molecules first interact with the surface of the lipid bilayer and consequently form weakly coupled oligomers. (C; left side): Micelles transform into fibril intermediates with the rate constant of $k_1$. The N- and C-terminal region of monomeric glucagon transform from α-helix to β-sheet structure in fibril form in the absence of bicelles. (C; right side): In the presence of lipid bilayers, weakly coupled oligomers transformed into fibril intermediate on the surface of bilelles with the rate constant of $k_1$. The N-terminal region remain the structure as α-helix, while the C-terminal region change the structure from α-helix to β-sheet. (D; left side): Fibril intermediates interact with monomeric glucagon to elongate the fibril in acetic acid solution with the rate constant of $k_2$. (D: right side) On the surface of lipid bilayers, fibril intermediates interact with monomeric glucagon to elongate the fibrils with the rate constant of $k_2$ and the longer fibrils protorude from the surface by taking same structures. Namely, the N-terminal region of glucagon fibril remains the structure to α-helix, while the C-terminal region changes the structure from α-helix to β-sheet. Throughout the diagram, types of β-sheet such as parallel or anti-parallel β-sheets have not been determined in this experiments.

**Table 2**
Rate constants for fibril nucleation ($k_1$) and fibril elongation ($k_2$) of two step autocatalytic reaction mechanism of glucagon in acetic acid solution in the absence and presence of bicelles.

| | Absence of bicelles | | Presence of bicelles | |
|---|---|---|---|---|
| | $k_1$ ($s^{-1}$) | $k_2$ ($s^{-1}M^{-1}$) | $k_1$ ($s^{-1}$) | $k_2$ ($s^{-1}M^{-1}$) |
| Gly4 ($1^{st}$) | $3.3 \times 10^{-8}$ | $1.7 \times 10^{-2}$ | $4.4 \times 10^{-6}$ | $3.1 \times 10^{-3}$ |
| Ala19 ($1^{st}$) | $2.0 \times 10^{-8}$ | $1.9 \times 10^{-2}$ | $3.8 \times 10^{-7}$ | $3.8 \times 10^{-3}$ |
| Gly4 ($2^{nd}$) | $3.3 \times 10^{-8}$ | $1.7 \times 10^{-2}$ | $2.1 \times 10^{-6}$ | $2.4 \times 10^{-3}$ |
| Ala19 ($2^{nd}$) | $2.0 \times 10^{-8}$ | $1.9 \times 10^{-2}$ | $2.1 \times 10^{-6}$ | $1.9 \times 10^{-3}$ |
| Av. RC ± σ* | (2.6 ± 0.7) X $10^{-8}$ | (1.8 ± 0.1) X $10^{-2}$ | (2.3 ± 1.4) X $10^{-6}$ | (2.8 ± 0.7) X $10^{-3}$ |

*Averaged rate constants (Av. RC) and standard deviations (σ) were obtained from averaging the values of Gly4 and Ala19 for two sets of time-course experiments.

obtained from the fibrillation process in the presence of bicelles is faster than that in the absence of bicelles, whereas the $k_2$ value obtained from the fibrillation process in the presence of bicelles is slower than that in the absence of bicelles. These results clearly indicate that lipid bilayers interact with glucagon molecules to alter the rate constants of fibril nucleation process as well as fibril elongation process.

## 4. Discussion

### 4.1. Conformational transition of glucagon from monomer to fibril

Conformation-dependent chemical shift values clearly indicate that the N-terminus of monomeric glucagon forms an α-helix structure, the center portion forms a random coil, and the C-terminus forms an α-helix structure as shown in Table 1 and Fig. 7 in acetic acid solution both in the presence and absence of bicelles. When the micelles aggregates to form fibrils, the N-terminal and C-terminal regions change from an α-helix to a β-sheet as seen with other amyloid-forming peptides in acetic acid solution in the absence of bicelles (left side of Fig. 7). In the presence of bicelles, the N-terminus forms an α-helix, the center portion forms a random coil, and the C-terminus forms an α-helix in the monomer state (right side of Fig. 7). In contrast to the case of glucagon in acetic acid solution, weakly coupled oligomers aggregate into fibrils in the presence of bicelles which results in the N-terminus maintaining an α-helix structure and the center portion remaining in a random coil structure, whereas the C-terminus changes from α-helix to β−sheet structure (right side of Fig. 7). There are therefore significant difference of structural transition between fibrils in the presence and absence of bicelles, with the N-terminus maintaining an α-helix structure in the process of fibril formation in the presence of bicelles. This result suggests that the N-terminal portion of glucagon fibril interacts with the lipid bilayer surface.

### 4.2. Fibrillation mechanism of glucagon in the presence and absence of bicelles

The above findings provide insights into the fibril-formation mechanism in the presence and absence of lipid bilayers as shown in Fig. 7. In the absence of lipid bilayers, monomers may aggregate with each other to form micelles as homogeneous reaction (Fig. 7B; left), likely driven by the amphipathic nature of the N-terminal and C-terminal α-helices. These micelles then change into a spherical fibril intermediates (Fig. 7C; left) as observed by TEM (Fig. 1A and B). Subsequently, this spherical fibril intermediate may form fibril nuclei and interact with monomeric glucagon to allow elongation of the fibril by changing from an α-helix to a β-sheet as a heterogeneous elongation process (Fig. 7D; left)

In the presence of lipid bilayers, monomer forms a structure similar to that in the absence of lipid bilayers. The monomer can likely associate quickly with a lipid bilayer, and subsequently associate with other monomers to form weakly coupled oligomers (Fig. 7B; right). These oligomers may change structure to form a fibril intermediate on the surface of the lipid bilayers to show elliptic shape fibril intermediates as shown in (Fig. 1E and Fig. 7C; right) on the surface of the lipid bilayer because the N-terminal structure retain an α-helix structure even in the fibril intermediates. The fibril intermediates grow into longer fibrils on the surface of the lipid bilayer and protrude outside the

lipid bilayers, as shown in the TEM image (Fig. 1F and G) and schematically shown in Fig. 7D; right.

The $k_1$ rate constant for nuclear formation in the presence of lipid bilayers is faster than in the absence of lipid bilayers because glucagon monomers associate with the surface of the lipid bilayer and then migrate laterally on the surface of the lipid bilayers to form weakly coupled oligomers and subsequently change to fibril intermediates as nucleation reaction. This two-dimensional process may be faster than the nuclear formation in the three-dimensional solution state.

The $k_2$ rate constant for fibril elongation in the presence of lipid bilayers is slower than in the absence of lipid bilayers. As discussed previously, the N-terminal part of glucagon molecules in fibrils in the presence of lipid bilayer remain in an α-helix. This α-helix may be stabilized when the helix interacts with the lipid bilayer. The stabilization of N-terminal α-helices in the presence of bicelles may slow down fibril elongation reaction with rate constant of $k_2$. It is reported that helical formation is critical for transition to β-structure (Abedin and Raleigh, 2009a,b). In case of glucagon, in the presence of bicelles, N-terminal α-helix becomes more stable due to the interaction with bicelles. This stability of N-terminal α-helix interacting with bicelles may affect to slow down the fibril elongation rate ($k_2$).This fibril can grow to the outside of the lipid bilayers because it potentially acts as a template to form structure identical to the fibril nuclei formed on the surface of the lipid bilayer. Because fibrils are interacting with lipid bilayers in the outside of the bicelles, the $k_2$ values for fibril elongation decrease as compared to the case in the absence of lipid bilayers.

It turned out that glucagon molecules significantly interact with lipid bilayers in the fibril formation processes. To understand the fibril formation process under physiological condition, a variety of lipid bilayer systems including lipid nanodiscs can be examined. These experimental results may gain insight into the mechanisms of glucagon fibril formation and cytotoxicity of glucagon fibrils in cell systems.

## 5. Conclusion

We demonstrated that glucagon forms fibrils in acetic acid solution in the absence of bicelles due to the N- and C- terminal regions of the molecule changing from an α-helix to a β-sheet structure. Glucagon also form fibrils in the presence of bicelles, with the N-terminus remaining its α-helix structure and the C-terminus changing the structure from an α-helix to a β-sheet. The kinetics of fibril formation can be explained by a two-step autocatalytic reaction mechanism. The rate constant of the nucleation process, $k_1$ of fibril formation in the presence of bicelles is faster than in the absence of bicelles due to the glucagon molecules being condensed on the surface of the lipid bilayer, thereby increasing the nucleation rate, $k_1$. On the other hand, the fibril elongation rate, $k_2$, is slower in the presence of bicelles because the N-terminal α-helices in the fibrils interact with lipid bilayers, thereby delay fibril elongation. Future work could be carried out at physiological pH with neutral bicelles and also with anionic bicelles. In addition, nanodiscs could be used as a model of lipid bilayers.

## Conflict of interest

The authors declare no conflict of interest.

## Acknowledgements

The authors thank Dr. Nakagoshi and Mr. Kondo in Yokohama National University for their help in obtaining the TEM images. This work was supported by Grants-in-Aid for Scientific Research in an Innovative Area from MEXT KAKENHI (Grant Numbers JP16H00756 to AN and JP16H00828 to IK), and by Grant-in-Aid for Scientific Research from JSPS KAKENHI (Grant Numbers JP15K06963 to AN and JP18H02387 to IK). AM acknowledge the internship program of Yokohama National University to stay in University of Melbourne (Laboratory of Prof. F. Separovic).

## Appendix A. Supplementary data

Supplementary material related to this article can be found, in the online version, at https://doi.org/10.1016/j.chemphyslip.2019.01.008.

## References

Abedin, A., Raleigh, D.P., 2009a. A role for helical intermediates in amyloid formation by natively unfolded polypeptides? Phys. Biol. 6, 015005.
Abedin, A., Raleigh, D.P., 2009b. A critical assessment of the role of helical intermediates in amyloid formation by natively unfolded proteins and polypeptides. Protein Eng. Des. Sel. 22, 453–459.
Bamaba, C., Ramamoorthy, A., 2018. Picturing the membrane-assisted choreography of cytochrome P450 with lipid-nanodiscs. Chem. Phys. Chem 11, 2603–2613.
Beaven, G.H., Gratzer, W.B., Davies, H.G., 1969. Formation and structure of gels and fibrils from glucagon. Eur. J. Biochem. 11, 37–42.
Bersch, B., Dörr, J.M., Hessel, A., Killian, J.A., Schanda, P., 2017. Proton-detected solid-state NMR spectroscopy of a zinc diffusion facilitator protein in native nanodiscs. Angew. Chem. Int. Ed. 56, 2508–2512.
Boesch, C., Bundi, A., Oppliger, M., Wüthrich, K., 1978. $^1$H nuclear-magnetic-resonance studies of the molecular conformation of monomeric glucagon in aqueous solution. Eur. J. Biochem. 91, 209–214.
Braun, W., Wider, G., Lee, K.H., Wüthrich, K., 1983. Conformation of glucagon in a lipid-water interphase by $^1$H nuclear magnetic resonance. J. Mol. Biol. 169, 921–948.
Brender, J.R., Salamekh, S., Ramamoorthy, A., 2012. Membrane disruption and early events in the aggregation of the diabetes related peptide IAPP from a molecular perspective. Acc. Chem. Res. 45, 454–462.
Bromer, W.W., Sinn, L.G., Behrens, O.K., 1957. The amino acid sequence of glucagon. V. Location of amide groups, acid degradation studies and summary of sequential evidence. J. Am. Chem. Soc. 79, 2807–2810.
Burke, M.J., Rougvie, M.A., 1972. Cross-β protein structures. I. Insulin fibrils. Biochemistry 11, 2435–2439.
Camargo, D.C.R., Korshavin, K.J., Jussupow, A., Raltchev, K., Goricanec, D., Fleisch, M., Sarkar, R., Xue, K., Aichler, M., Mettenleiter, G., Walch, A.K., Camilloni, C., Hagn, F., Reif, B., Ramamoorthy, A., 2017. Stabilization and structural analysis of a membrane-associated hIAPP aggregation intermediate. eLIFE 6, e31226.
Chimon, S., Shaibat, M.A., Jones, C.R., Calero, D.C., Aizezi, B., Ishii, Y., 2007. Evidence of fibril-like β-sheet structures in a neurotoxic amyloid intermediate of Alzheimer's β-amyloid. Nat. Struct. Mol. Biol. 14, 1157–1174.
Colvin, M.T., Silvers, R., Ni, Q.Z., Can, T.V., Sergeyev, I., Rosay, M., Donovan, K.J., Michael, B., Wall, J., Linse, S., Griffin, R.G., 2016. Atomic resolution structure of monomorphic $A\beta_{42}$ amyloid fibrils. J. Am. Chem. Soc. 138, 9663–9674.
Cooper, G.J.S., Willis, A.C., Clark, A., Turner, R.C., Sim, R.B., Reid, K.B.M., 1987. Purification and characterization of a peptide from amyloid-rich pancreases of type 2 diabetic patients. Proc. Natl. Acad. Sci. U. S. A. 84, 8628–8632.
Denisov, I.G., Sligar, S.G., 2017. Nanodiscs in membrane biochemistry and biophysics. Chem. Rev. 117, 4669–4713.
Gorman, P.M., Chakrabartty, A., 2001. Alzheimer β-amyloid peptides; structures of amyloid fibrils and alternate aggregation products. Biopolymers 60, 381–394.
Itoh-Watanabe, H., Kamihira-Ishijima, M., Javkhlantugs, N., Inoue, R., Itoh, Y., Endo, H., Tuzi, S., Saitô, H., Ueda, K., Naito, A., 2013a. Role of aromatic residues in amyloid fibril formation of human calcitonin by solid-state $^{13}$C NMR and molecular dynamics simulation. Phys. Chem. Chem. Phys. 15, 8890–8901.
Itoh-Watanabe, H., Kamihira-Ishijima, M., Kawamura, I., Kondoh, M., Nakakoshi, M., Sato, M., Naito, A., 2013b. Characterization of the spherical intermediates and fibril formation of hCT in HEPES solution using solid-state $^{13}$C-NMR and transmission electron microscopy. Phys. Chem. Chem. Phys. 15, 16956–16964.
Kael, M.A., Weber, D.K., Separovic, F., Sami, M.A., 2018. Aggregation kinetics in the presence of brain lipids of Aβ(1-40) cleaved from a soluble fusion protein. Biochim. Biophys. Acta 1860, 1681–1689.
Kamgar-Parsi, K., Tolchard, J., Habenstein, B., Loquet, A., Naito, A., Ramamoorthy, A., 2017a. Structural biology of calcitonin: from aqueous therapeutic properties to amyloid aggregation. ISR. J. Chem. 57, 634–650.
Kamgar-Parsi, K., Hong, L., Naito, A., Brooks 3rd, C.L., Ramamoorthy, A., 2017b. Growth-incompetent monomers of human calcitonin lead to a noncanonical direct relationship between peptide concentration and aggregation lag time. J. Biol. Chem. 292, 14963–14976.
Kamihira, M., Naito, A., Tuzi, S., Nosaka, A.Y., Saitô, H., 2000. Conformational transition and fibrillation mechanism of human calcitonin as studied by high-resolution solid-state $^{13}$C NMR. Protein Sci. 9, 867–877.
Knowles, T.J., Finka, R., Smith, C., Lin, Y.-P., Daffom, T., Overduin, M., 2009. Membrane proteins solubilized intact in lipid containing nanoparticles bounded by styrene maleic acid copolymer. J. Am. Chem. Soc. 131, 7484–7485.
Košmrlj, A., Cordsen, P., Kyrsting, A., Otzen, D.E., Oddershede, L.B., Jensen, M.H., 2015. A. Monomer-trimer model supports intermittent glucagon fibril growth. Sci. Rep. 5, 9005.
Kotler, S.A., Walsh, P., Brender, J.R., Ramamoorthy, A., 2014. Difference between amyloid-β aggregation in solution and on the membrane: insights into elucidation of the mechanistic details of Alzheimer's disease. Chem. Soc. Rev. 43, 6692–6700.
Matsuzaki, K., 2014. How do membranes initiate Alzheimer's disease? Formation of toxic amyloid fibrils by the amyloid β-protein on ganglioside clusters. Acc. Chem. Res. 47,

2397–2404.
Naito, A., Kawamura, I., 2007. Solid-state NMR as a method to reveal structure and membrane-interactions of amyloidogenic protein and peptide. Biochim. Biophys. Acta 1768, 1900–1912.
Okada, Y., Okubo, K., Ikeda, K., Yanao, Y., Hoshino, M., Hayashi, Y., Kiso, Y., Itho-Watanabe, H., Naito, A., Matsuzaki, K., 2018. Toxic amyloid tape: A novel mixed antiparallel/parallel β-sheet structure formed by amyloid b-protein on GM1 clusters. ACS Chem. Neurosci. https://doi.org/10.1021/acschemneuro.8b00424.
Onoue, S., Ohshima, K., Debari, K., Koh, K., Shioda, S., Iwasa, S., Kashimoto, K., Yajima, T., 2004. Mishandling of the therapeutic peptide glucagon generates cytotoxic amyloidogenic fibrils. Pharm. Res. 21, 1274–1283.
Onoue, S., Iwasa, S., Kojima, T., Katoh, F., Debari, K., Koh, K., Matsuda, Y., Yajima, T., 2006. Structural transition of glucagon in the concentrated solution observed by electrophoretic and spectroscopic techniques. J. Chromatogr. A 1109, 167–173.
Paquet, A., 1982. Introduction of 9-fluorenylmrthyloxycarbonyl, trichloroethoxy-carbonyl and benzyloxycarbonyl amine protecting groups into O-unprotected hydroxyamino acids using succinimidyl carbonates. Can. J. Chem. 60, 976–980.
Pedersen, J.S., Dikov, D., Flink, J.L., Hijuler, H.A., Christiansen, G., Otzen, D.E., 2006. The changing face of glucagon fibrillation: structural polymorphism and conformational imprinting. J. Mol. Biol. 355, 501–523.
Petkova, A.T., Yan, W.M., Tycko, R., 2006. Experimental constraints on quaternary structure in Alzheimer's β-amyloid fibrils. Biochemistry 45, 498–512.
Pohl, S.I., Birnbaumer, L., Rodbell, M., 1969. Glucagon-sensitive adenyl cyclase in plasma membrane of hepatic parenchymal cells. Science 164, 566–567.
Prusiner, S.B., 1998. Prions. Proc. Natl. Acad. Sci. U. S. A. 95, 13363–13383.
Ravula, T., Hardin, N.Z., Ramadugu, S.K., Cox, S.J., Ramamoorthy, A., 2018. Formation of pH-resistant monodispersed polymer-lipid nanodiscs. Angew. Chem. Int. Ed. 57, 1342–1345.
Rodbell, M., Birnbaumer, I., Pohl, S.L., Sundby, F., 1971. The reaction of glucagon with its receptor: evidence for discrete regions of activity and binding in the glucagon molecule. Proc. Natl. Acad. Sci. U. S. A. 68, 909–913.
Sahoo, B.R., Genjo, T., Cox, S.J., Stoddard, A.K., Anantharamaiah, G.M., Fierke, C., Ramamoothy, A., 2018a. Nanodisc-forming scaffold protein promoted retardation of amyloid-beta aggregation. J. Mol. Biol. 430, 4230–4244.
Sahoo, B.R., Genjo, T., Bekier II, M., Cox, S.J., Stoddard, A.K., Ivanova, M., Yasuhara, K., Fierke, C.A., Wang, Y., Ramamoorthy, A., 2018b. Alzheimer's amyloid-beta intermediates generated using polymer-nanodiscs. Chem. Comm. 54, 12883–12886.
Saitô, H., 1986. Conformation-dependent $^{13}C$ chemical shifts: a new means of conformation characterization as obtained by high-resolution solid-state $^{13}C$ NMR. Magn. Reson. Chem. 74, 196–200.
Saitô, H., Ando, I., 1989. High-resolution solid-state NMR studies of synthetic and biological macromolecules. Annu. Rep. NMR Spectrosc. 21, 209–290.
Saitô, H., Ando, I., Ramamoorthy, A., 2010. Chemical shift tensor – the heart of NMR: insight into biological aspect proteins. Prog. Nucl. Magn. Reson. Spectrosc. 57, 181–228.
Sanders II, Charles R., Schwonek, J.P., 1992. Characterization of magnetically orientable bilayers in mixtures of dihexanoylphosphatidylcholine and dimyristoylphosphatidylcholine by solid-state NMR. Biochemistry 31, 8898–8905.
Sasaki, K., Dockerill, S., Adamiak, D.A., Tickle, I.J., Blundell, T., 1975. X-ray analysis of glucagon and its relationship to receptor binding. Nature 257, 751–757.
Schaefer, J., Sejeskal, E.O., 1976. Carbon-13 nuclear magnetic resonance of polymers spinning at magic angle. J. Am. Chem. Soc. 98, 1031–1032.
Scherzinger, E., Lurz, R., Turmaine, M., Mangiarini, L., Hollenbach, B., Hasenbank, R., Bates, G.P., Davies, S.W., Lehrach, H., Wanker, E.E., 1997. Huntington-encoded polyglutamine expansions from amyloid-like protein aggregates in vitro and in vivo. Cell 90, 549–558.
Sipe, J.D., 1992. Amyloidosis. Annu. Rev. Biochem. 61, 947–975.
Sipe, J.D., Cohen, A.S., 2000. History of the amyloid fibril. J. Struct. Biol. 130, 88–98.
Thomaier, M., Gremer, L., Dammers, C., Fabig, J., Neudecker, P., Willbold, D., 2016. High-affinity binding of monomeric but not oligomeric amyloid-β to ganglioside GM1 containing nanodiscs. Biochemistry 55, 6662–6672.
Tycko, R., 2003a. Insight into the amyloid folding problem from solid-state NMR. Biochemistry 42, 3151–3159.
Tycko, R., 2003b. Application of solid state NMR to the structural characterization of amyloid fibrils: methods and results. Prog. NMR Spectrosc. 42, 53–68.
Vines, G., 1993. Alzheimer's disease – from cause to cure? Trends Biotechnol. 11, 49–55.
Wälti, M.A., Ravotti, F., Arai, H., Glabe, C.G., Wall, J.S., Böckmann, A., Güntert, P., Meier, B.H., Riek, R., 2016. Atomic-resolution structure of a disease-relevant Aβ(1-42) amyloid fibril. Proc. Natl. Acad. Sci. U. S. A. 113, E4976–E4984.
Xiao, Y., Ma, B., McElheny, D., Parthasarathy, S., Long, F., Hoshi, M., Nussinov, R., Ishii, Y., 2015. Aβ(1-42) fibril structure illuminates self-recognition and replication of amyloid in Alzheimer's disease. Nat. Struct. Mol. Biol. 22, 499–505.
Yamamoto, K., Gildenberg, M., Ahuja, S., Im, S.-C., Pearcy, P., Waskell, L., Ramamoorthy, A., 2013. Probing the transmembrane structure and topology of microsomal cytochrome-P450 by solid-state NMR on temperature-resistant bicelles. Sci. Rep. 3, 2556.
Zhang, M., Huang, R., Ackermann, R., Im, S.-C., Waskell, L., Schwendeman, A., Ramamoorthy, A., 2016. Reconstitution of the Cytb5-CytP450 complex in nanodiscs for structural studies using NMR spectroscopy. Angew. Chem. Int. Ed. 55, 4497–4499.